Decomposition of NH_3 on Ir(100): A Temperature Programmed Desorption Study

A. K. Santra, B. K. Min, C. W. Yi, Kai Luo, T. V. Choudhary, and D. W. Goodman*

Department of Chemistry, Texas A&M University, P.O. Box 30012, College Station, Texas 77840-3012

Received: June 19, 2001; In Final Form: September 27, 2001

Ammonia adsorption has been studied on an Ir(100) surface in the temperature range 100−410 K. In contrast to previous studies on Ir(111), approximately 12% of the chemisorbed ammonia undergoes stepwise decomposition at 200 K. However, decomposition has been found to be an activated process wherein a difference in the activation energy of dissociation and desorption is estimated to be 21 kJ/mol. Recombinative nitrogen desorption, occurring at temperature as low as 500 K, has been found to be the crucial step for having continuous and efficient ammonia decomposition with an activation energy of 64 kJ/mol. Coadsorption of hydrogen and ammonia have been carried out to understand the partial pressure dependences for ammonia decomposition---0.9 ± 0.1 with respect to ammonia and -0.7 ± 0.1 with respect to hydrogen. Coadsorption data indicate that the negative order with respect to hydrogen is due to enhancement of the reverse reaction ($NH_x + H \rightarrow NH_{x+1}$, $x = 0-2$) as well as reduction in the desorption temperature of ammonia in the presence of excess H-atoms on the surface. In contrast, coadsorbed oxygen acts as a promoter for the ammonia dissociation and leads to 100% ammonia conversion. The differences in the decomposition behavior with respect to the previous results for Ir(111) are indicative of the structure sensitivity of the reaction.

Introduction

Due to the increasing demand for efficient and nonpolluting energy alternatives to conventional energy sources, fuel cells have received considerable attention in recent years. In this regard, low-temperature fuel cells are of great interest, yet require CO_x-free hydrogen for optimum operation. For example, proton exchange membrane fuel cells can tolerate only ppm levels of CO in the hydrogen fuel, whereas alkaline fuel cells require CO_x-free hydrogen. Conventional hydrogen production technologies such as steam reforming, partial oxidation, and autothermal reforming of hydrocarbons produce large amounts of CO_x as byproducts.[1,2] Removal of CO_x from the hydrogen stream to ppm levels adds considerable complexity to the process, imposing serious limitations to its use in vehicular and small-scale fuel cell applications. These limitations to the existing conventional hydrogen production technologies are the motivation for exploration of CO_x-free alternatives for hydrogen production.[3−6] One obvious alternative to CO_x-free hydrogen production is the catalytic decomposition of ammonia.

The decomposition of ammonia ($NH_3 \rightarrow {}^1/_2N_2 + {}^3/_2H_2$) is an endothermic process ($\Delta H = +46.4$ kJ/mol). Ammonia adsorption and decomposition has been studied on Al,[7] Fe,[8] Re,[9] Rh,[10] Ni,[11] Pt,[12−14] Ru,[15] and W[16] single-crystal surfaces. The general consensus is that recombinative desorption of N_2 is the rate-limiting step. Early transition metals are very active for ammonia decomposition, however, typically these metals are limited by their relatively high recombinative nitrogen desorption temperature or their tendency to deactivate via nitride formation. Critical to an optimum ammonia decomposition catalyst is a low recombinative desorption temperature for N_2 since this step is recognized to be the rate-determining step. Pt and Ir offer comparable temperatures for recombinative nitrogen desorption with acceptable activities. Our preliminary data for ammonia decomposition on high surface area Ir/SiO_2 and Ir/Al_2O_3 show that these catalysts are very effective.[17] More interestingly, the interaction of NH_3 with metal wires of Pd, Ir, Pt, and Rh has been investigated recently in a differential flow reactor and Ir shown to be the most efficient catalyst.[18] Surprisingly, there are no reports in the literature of ammonia decomposition on Ir single-crystal surfaces. On Ir(111), NH_3 was found to adsorb molecularly, nitrogen-end down with C_{3V} symmetry via angle-resolved photoemission.[19] The adsorption of ammonia on Pt single-crystal surfaces has been extensively investigated.[12−14] Among the Pt single-crystal surfaces, ammonia decomposition occurs on the more-open (1 × 1) surface of Pt(100),[13] whereas the close-packed (1 × 5) or more known as (100)-hex surface is inert with respect to decomposition. On the other hand, comparative NH_3 adsorption experiments[14] on Pt(111), (100)-hex, (110), (210), and (211) have shown no dissociation and the conclusion reached that the binding strength of NH_3 does not depend significantly on the particular crystal plane.

A comprehensive understanding of ammonia decomposition depends critically upon understanding the interaction of the reaction products, hydrogen and nitrogen, with the metal catalyst in question. A molecular beam study[20] of hydrogen adsorption on Ir(100) shows two desorption features on the reconstructed, close-packed, pseudohexagonal (1 × 5) surface, whereas the unreconstructed, open, metastable (1 × 1) surface exhibits only one peak. The nitrogen desorption temperatures on the (1 × 5) surface are 240 and 400 K for the α and β species, respectively, while on the (1 × 1) surface, nitrogen desorption occurred near 400 K. Coadsorption of hydrogen with CO and K has been studied[21] on Ir single-crystal surfaces. Very recently, multilayer-induced decomposition of hydrocarbons also has been observed on Ir(111).[22] Nitrogen adsorption on the Ir(111) surface, studied with high-resolution electron energy loss spectroscopy (HREELS) and temperature programmed desorption (TPD), found N_2 to adsorb reversibly and molecularly below 200 K.[23] Here we report a detailed investigation of NH_3 and $N^{15}D_3$ adsorption on Ir(100) in the presence and absence of coadsorbed hydrogen.

Experimental Section

The experiments were carried out in an ultrahigh vacuum (UHV) chamber (base pressure of $<2 \times 10^{-10}$ Torr) equipped with Auger electron spectroscopy (AES), ion scattering spec-

* Corresponding author. Tel.: (979) 845-0214. Fax: (979) 845-6822. E-mail: goodman@mail.chem.tamu.edu.

10.1021/jp0123132 CCC: $22.00
Published on Web 12/14/2001

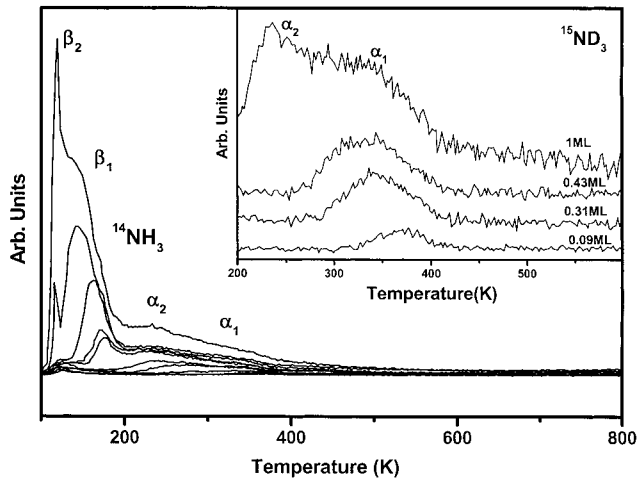

Figure 1. TPD of $^{14}NH_3$ for various exposures at 100 K. The inset shows the TPD of $^{15}ND_3$ for submonolayer to monolayer coverages at 200 K.

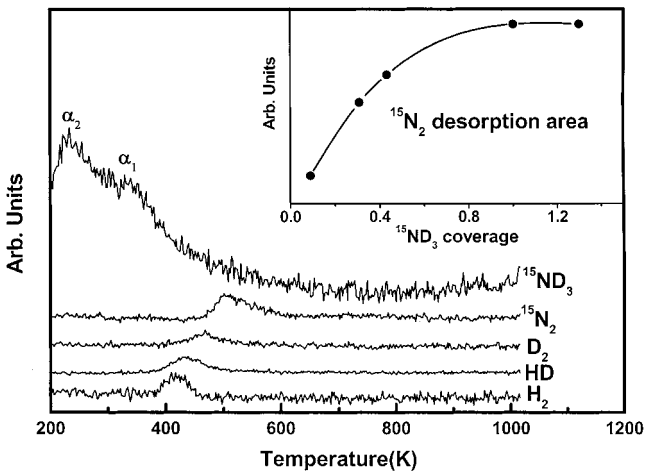

Figure 2. TPD spectra of m/e = 2, 3, 4, 21, and 30 from a 1ML $^{15}ND_3$ adsorbed Ir(100) surface at 200 K. Inset shows a plot of the integrated intensity under the $^{15}N_2$ desorption peak for various ammonia exposures.

troscopy (ISS), X-ray photoelectron spectroscopy (XPS), and TPD.[24] The Ir(100) crystal was cleaned by argon sputtering and repeated cycles of heating in O_2 ($P = 1 \times 10^{-7}$ Torr; 15 min) with a subsequent anneal to 1500 K until no C and O signals were detectable with XPS. Anhydrous NH_3 (99.99%, Matheson) and $^{15}ND_3$ (Icon Isotopes, ^{15}N/99% and D/98%) were further purified by freeze−pump−thaw cycles; hydrogen (99.999%, Matheson) was cleaned by passing it through a liquid nitrogen cooled trap. The crystal was mounted on a Ta sample holder (dia.:0.0255 cm); the temperature of the sample was monitored with a W-5%Re/W-26%Re thermocouple spot-welded to the back of the sample. TPD experiments were carried out using a UTI quadrupole mass spectrometer with a heating rate of 5 K/s. Since variations in TPD spectra have been observed due to electron beam effects,[11] TPD spectra were acquired while biasing the crystal at −100 V; no differences in the TPD data were seen. In the $^{15}ND_3$ experiments, desorption due to $^{15}ND_2H$, $^{15}NDH_2$, and $^{15}NH_3$ was observed resulting presumably from the isotopic exchange of ammonia with background hydrogen. For simplicity, we have shown only spectra due to $^{15}ND_3$(m/e = 21). It is noteworthy that each of the three isomers has identical spectral shapes and desorption temperatures. For quantitative purposes, we have taken the total integrated area under the desorption peaks of all the species.

Results and Discussion

Thermal desorption of $^{14}NH_3$ was measured with increasing exposures of $^{14}NH_3$ at an adsorption temperature of 100 K on Ir(100) as shown in Figure 1. At the lowest $^{14}NH_3$ coverage measured, a single desorption peak, designated as α_1-NH_3, is seen near 370 K. As the coverage is increased, a new feature at ca. 235 K appears and is designated as α_2-NH_3. The desorption process completes with the sequential development of two very distinct peaks below 200 K, designated as β_1- and β_2-NH_3. The adsorption behavior is very similar to that observed on Ru(001)[15] and Re(0001)[9] where the α_1 and α_2 species are known to represent completion of the first monolayer while the β_1 and β_2 species correspond to multilayer formation. In addition to the desorption of molecular ammonia, m/e = 2 (H_2) and 28 (N_2) are found, indicative of ammonia decomposition. Because of the mass ambiguity of CO (m/e = 28) and NH_3, $^{15}ND_3$ and $^{14}NH_3$ have been used for clarity. For simplicity, only the $^{15}ND_3$ data are discussed, although the TPD spectra recorded for $^{14}NH_3$ show precisely the same behavior. The inset of Figure 1 shows the desorption behavior for molecular $^{15}ND_3$ at submonolayer coverages up to a monolayer. The appearance of only the α_1 species at 0.09ML is apparent, whereas the desorption temperature shifts toward low temperature (340 K) with increasing surface coverage due to the intermolecular repulsion. At 0.43ML exposure the α_2 species appears and shifts toward lower desorption temperatures as the coverage increases for the same reason as discussed for the α_1 species.

In Figure 2 typical desorption spectra for H_2, HD, D_2, $^{15}N_2$ and $^{15}ND_3$ from a 1ML $^{15}ND_3$ covered surface are shown after exposure at 200 K. A very small H_2 desorption peak at ca. 420 K from background adsorption is apparent. The detailed behavior of hydrogen desorption will be discussed later in the text. Interestingly, the desorption temperature of HD (435 K) and D_2 (470 K) differ by about 35 K and appear at a higher temperature than that of background H_2. The desorption temperature of recombinative $^{15}N_2$ is even higher (510 K). Since all three species are related to the decomposition of $^{15}ND_3$, one can conclude that the decomposition of ammonia occurs in a stepwise manner and recombinative desorption of $^{15}N_2$ is the last and crucial step for having continuous ammonia decomposition. Since the high-temperature tail of the α_1 species (400−500 K) appears concomitantly with those of HD and D_2, we attribute this tail to recombinative desorption of $^{15}ND_3$ due to the reverse reaction (step 2: i.e., $^{15}ND_2 + D \rightarrow {}^{15}ND_3$) of the generally accepted reaction scheme:[8]

$$^{15}ND_3(g) \rightarrow {}^{15}ND_3(a) \quad (1)$$

$$^{15}ND_3(a) \rightarrow {}^{15}ND_2(a) + D(a) \quad (2)$$

$$^{15}ND_2(a) \rightarrow {}^{15}ND(a) + D(a) \quad (3)$$

$$^{15}ND(a) \rightarrow {}^{15}N(a) + D(a) \quad (4)$$

$$^{15}N(a) + {}^{15}N(a) \rightarrow {}^{15}N_2(g) \quad (5)$$

$$D(a) + D(a) \rightarrow D_2(g) \quad (6)$$

In the inset of Figure 2 the area under the $^{15}N_2$ desorption curves is plotted for various ammonia doses. These data show that a saturation level is reached following a monolayer dose and that no multilayer induced dissociation occurs as has been seen on

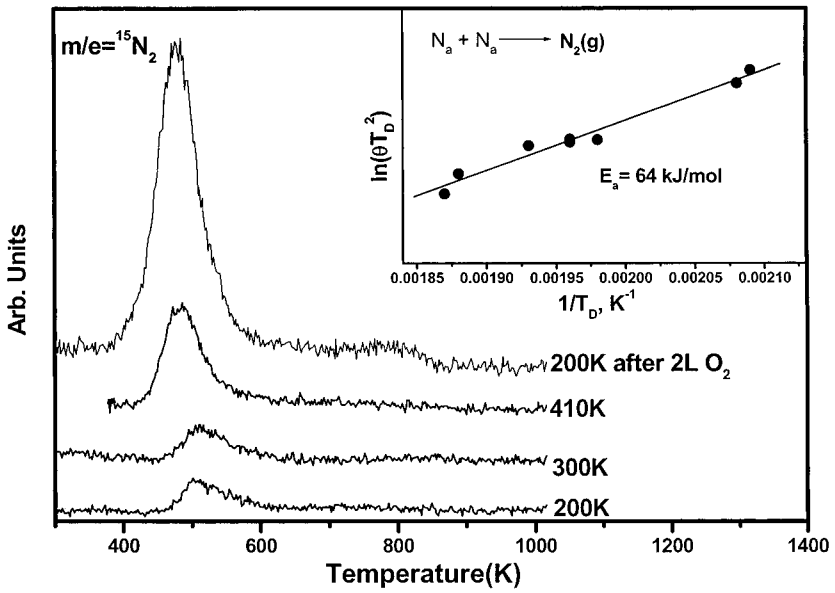

Figure 3. TPD of $^{15}N_2$ at various ammonia adsorption conditions. Inset shows the activation energy estimated using the Redhead equation and second-order recombinative desorption kinetics for nitrogen.

an Ir single-crystal surface for hydrocarbon adsorption.[22] The fraction of ammonia dissociation is approximately 12%.

To check whether ammonia dissociation is an activated process, ammonia was exposed to the Ir(100) surface at various temperatures. The resulting TPD spectra of $^{15}N_2$ are shown in Figure 3. A marked increase in the amount of $^{15}N_2$ desorption is apparent as the surface temperature is increased to 410 K. In fact, the amount of $^{15}N_2$ desorption gradually increases from 300 to 410 K with an increase in the adsorption temperature, indicating that ammonia dissociation is an activated process. From an Arrhenious plot the activation energy (E_{diff}) is estimated to be 21 kJ/mol. As is evident in the inset of Figure 1, the desorption temperature of ammonia (360 K) is comparable to the temperature for its activated dissociation (300−410 K), therefore it is reasonable to assume that desorption of ammonia and dissociation are very competitive. Thus the observed 5 kcal/mol activation energy barrier can be attributed to the difference in the activation energy for desorption and that for dissociation ($E_{diff} = E_{diss} - E_{desorp}$). This approximation has been applied recently to ammonia decomposition on Ni.[10] Since E_{diff} is a positive number, to increase the probability of dissociation the desorption temperature must be increased to enhance the retention time of ammonia on the surface such that decomposition can occur prior to desorption. To confirm this premise, a monolayer of $^{15}ND_3$ was adsorbed at 200 K on a 2L O_2 (<0.1ML) preadsorbed surface.

Indeed an order of magnitude increase in the dissociation of ammonia with 100% conversion was observed; no desorption of ammonia was seen. This marked enhancement of the dissociation activity could arise because of the following: (a) abstraction of D atoms [$^{15}ND_3(a) + O(a) \rightarrow {}^{15}ND_2(a) + OD(a)$], leading to desorption of D_2O as an additional product and/or (b) an increase in the desorption temperature of $^{15}ND_3$(a). An increase in the desorption temperature of ammonia is anticipated because: (a) a surface complex of the type $^{15}ND_3(a)-O_a$ might form; and (b) the oxygen adatoms can result in an electron-deficient Ir surface such that electron donation (σ type) from ammonia is now more favorable, increasing the metal−ammonia binding strength. Only a very small amount of water desorption was apparent from this surface, consistent with an enhanced dissociation activity, and is due mainly to the increase in the desorption temperature of ammonia. Therefore the electronegative character of oxygen makes it a promotor for ammonia dissociation. This oxygen-induced enhancement of ammonia dissociation has been observed as well for Ni(110).[25] The activation energy using the Redhead equation[26] and assuming second-order kinetics for the recombinative nitrogen desorption is estimated to be 64 kJ/mol (shown in the inset of Figure 3).

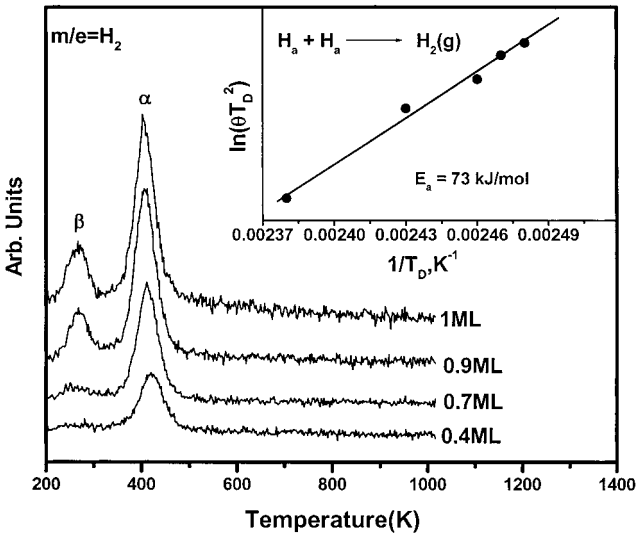

Figure 4. TPD of H_2 at various exposures of hydrogen on Ir(100). Inset shows the activation energy plot estimated using the Redhead equation and second-order recombinative desorption kinetics for hydrogen.

Recent high-pressure kinetics data[27] in our laboratory for ammonia decomposition on Ir(100) show that the order of the reaction is positive (0.9) with respect to ammonia and negative (−0.7) with respect to hydrogen. Since hydrogen is one of the reaction products it is essential to understand the influence of hydrogen. Accordingly, experiments of hydrogen coadsorbed with ammonia were carried out. Prior to discussion of the coadsorption results it is instructive to describe the adsorption of hydrogen alone. In Figure 4 the TPD of hydrogen is shown with increasing hydrogen coverage on an Ir(100) surface. At low coverage (up to 0.7ML) only one desorption feature is apparent at ca. 410 K while a second low temperature feature

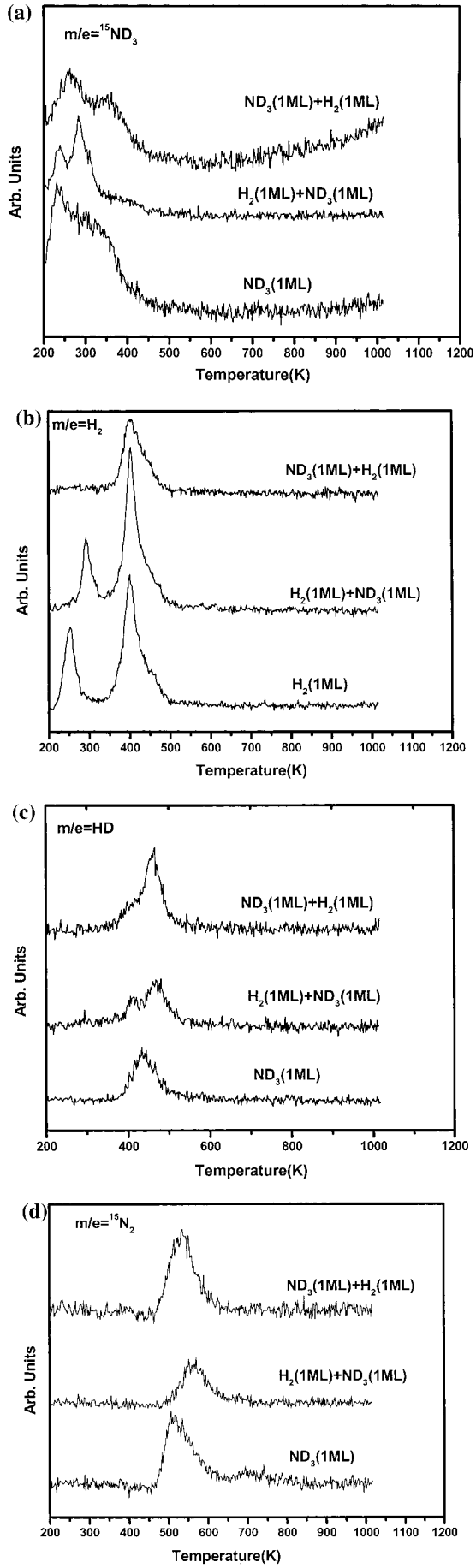

Figure 5. TPD from a IML $^{15}ND_3$, H_2 (1ML) followed by $^{15}ND_3$(1ML) and vice versa for (a) $m/e = {}^{15}ND_3$, (b) $m/e = H_2$, (c) $m/e =$ HD, and (d) $m/e = {}^{15}N_2$.

at ca. 270 K appears with further adsorption. The desorption behavior is in excellent agreement with previously reported data[20] where the high-temperature peak was assigned to atomic hydrogen (α) adsorbed on a hydrogen-induced reconstructed (1×1) surface and the low-temperature peak (β) to that for an unreconstructed (5×1) surface. Using second-order[26] kinetics the activation energy for recombinative desorption of hydrogen is calculated to be 73 kJ/mol, comparable to the literature value. Although the desorption temperature of molecular hydrogen is slightly lower than that of nitrogen, the activation energy of recombination of hydrogen (Figure 4) is 9 kJ/mol higher than the latter (Figure 3); this could be explained by assuming hydrogen to have a relatively higher preexponential factor.

Coadsorption experiments were carried out by first adsorbing hydrogen, then ammonia and vice versa. Figure 5a shows the $^{15}ND_3$ desorption TPD from three different surfaces. The hydrogen-preadsorbed surface shows two very sharp desorption features at ca. 240 and 290 K. The high temperature feature is much sharper for the hydrogen preadsorbed surface than for hydrogen alone and the desorption occurs at a lower temperature than for clean Ir(100). However, for hydrogen adsorbed after ammonia, the desorption features for hydrogen appear very similar to those from the clean surface, except the peaks are now shifted toward higher temperatures. The reason for these dramatic changes is not clear; however, obviously different lateral interactions arise due to preferential site occupation of ammonia and hydrogen that is strongly dependent upon the dosing sequence. In Figure 5b is shown the TPD for H_2 desorption from a hydrogen-preadsorbed surface, where the weakly adsorbed β-peak (295 K) is now shifted toward a higher temperature compared to the clean surface (270 K). This shift suggests a lateral interaction between hydrogen and coadsorbed ammonia (consistent with the lower ammonia desorption temperature of Figure 5a). However, the high-temperature feature (410 K, α) remains unperturbed. Interestingly, when ammonia was adsorbed prior to hydrogen, no weakly adsorbed β-peak was observed, indicating that either ammonia molecules are blocking the close-packed (5×1) sites of Ir(100) or that preadsorption of ammonia leads to complete reconstruction of the (5×1) surface to a (1×1) surface. It is noteworthy that on a (1×1) reconstructed surface only the strongly adsorbed α-peak was observed.[20] Considering the HD desorption TPD of Figure 5c, a new peak is apparent at lower temperature (410 K) while the original feature (440 K) on the clean surface has shifted toward a higher desorption temperature (470 K). The new low-temperature feature appears at the same temperature as the α-peak of H_2, consistent with isotopic exchange with the D-atoms from ammonia decomposition. The high-temperature shift of the original HD peak (440 K) due to ammonia decomposition can be attributed to a change in the dissociation temperature of ammonia. In Figure 5d, the $^{15}N_2$ desorption features show similar shifts toward higher temperature upon coadsorption of hydrogen. From the hydrogen preadsorbed surface we see a slight decrease in the extent of dissociation. Therefore, from the coadsorption data we conclude that the excess coverage of hydrogen can: (i) interact laterally with the adsorbed ammonia and promote the desorption of ammonia at a lower temperature than that from the clean surface, contrary to coadsorbed oxygen (Figure 4); and (ii) accelerate the reverse reactions ($^{15}ND_x + H \rightarrow {}^{15}ND_xH$, $x = 0-2$), such that the onset of dissociation is at a slightly higher temperature. Therefore the negative order with respect to hydrogen observed in our high-pressure kinetic experiments is due to the weaker bonding of ammonia in the presence of excess H-atoms on the surface

which, in turn, favors the backward reactions ($^{15}ND_x + H \rightarrow {}^{15}ND_xH$, $x = 0-2$), i.e., desorption of ammonia instead of dissociation.

Conclusions

1. In contrast to the behavior observed on Ir(111), ammonia decomposition occurs in a stepwise manner on the Ir(100) surface even at UHV conditions and adsorption temperatures as low as 200 K.

2. Recombinative nitrogen desorption occurs below 500 K with an activation energy of 64 kJ/mol, comparable to the apparent activation energy of 84 and 82 kJ/mol estimated in our high pressure study on Ir(100)[26] and Ir/Al_2O_3,[17] respectively. This is the crucial step for having efficient ammonia decomposition in a continuous manner at lower temperature.

3. Desorption and dissociation of ammonia is found to be very competitive; the difference in the activation energy of desorption and dissociation is estimated to be 21 kJ/mol.

4. Hydrogen adsorption data are in excellent agreement with those reported in the literature on Ir(100).

5. Coadsorption of hydrogen and ammonia are consistent with recent high-pressure ammonia decomposition results yielding negative order (−0.7) with respect to the hydrogen partial pressure.[27]

6. Coadsorbed oxygen has been found to act as a promoter for ammonia decomposition by electronically modifying the surface, thereby increasing the desorption temperature of ammonia.

Acknowledgment. We acknowledge with pleasure the support of this work by the Department of Energy, Office of Basic Energy Sciences, Division of Chemical Sciences.

References and Notes

(1) Rostrup-Nielsen, J. R. In *Catalytic Steam Reforming, Science and Engineering*; Anderson, J. R., Boudart, M., Eds.; Springer: Berlin, 1984; Vol. 5.

(2) Armor, J. N. *Appl. Catal.* **1999**, *176*, 159.

(3) Choudhary, T. V.; Goodman, D. W. *Catal. Lett*. **1999**, *59*, 93.

(4) Choudhary, T. V.; Goodman, D. W. *J. Catal*. **2000**, *192*, 316.

(5) Choudhary, T. V.; Sivadinarayana, C.; Chusuei, C.; Klinghoffer, A.; Goodman, D. W. *J. Catal.* **2001**, *199*, 9.

(6) Choudhary, T. V.; Sivadinarayana, C.; Klinghoffer, A.; Goodman, D. W. *Stud. Surf. Sci. Catal.* **2001**, *136*, 197.

(7) Kim, C. S.; Bermudez, V. M.; Russel, J. N., Jr. *Surf. Sci.* **1997**, *389*, 162.

(8) Ertl, G.; Huber, M. *J. Catal.* **1980**, *61*, 537.

(9) Rosenzweig, Z.; Asscher, M. *Surf. Sci.* **1990**, *225*, 249.

(10) Metkemeijer, R.; Achard, P. *Int. J. Hydrogen Energy* **1994**, *19*, 535.; *J. Power Sources* **1994**, *49*, 271.

(11) Bassignana, I. C.; Wagemann, K.; Kuppers, J.; Ertl, G. *Surf. Sci*. **1986**, *175*, 22; Huttinger, M.; Kuppers, J. *Surf. Sci.* **1983**, *130*, L277; Chrysostomou, D.; Flowers, J.; Zaera, F. *Surf. Sci*. **1999**, *439*, 34.

(12) Tsai, W.; Vajo, J. J.; Weinberg, W. H. *J. Phys. Chem.* **1985**, *89*, 4926; Vajo, J. J.; Tsai, W.; Weinberg, W. H. *J. Phys. Chem*. **1986**, *90*, 6531; *ibid* **1985**, *89*, 3243; Loffler, D. G.; Schmidt, L. D. *Surf. Sci.* **1976**, *59*, 195.

(13) Bradeley, J. M.; Hopkinson, A.; King, D. A. *Surf. Sci*. **1997**, *371*, 255.

(14) Gohndrone, J. M.; Olsen, C. W.; Backman, A. L.; Gow, T. R.; Yagasaki, E.; Masel, R. I. *J. Vac. Sci. Technol*. **1989**, *7*, 1986.

(15) Sun, Y. K.; Wang, Y. Q.; Mullin, C. B.; Weinberg, W. H. *Langmuir* **1991**, *7*, 1689; Tsai, W.; Weinberg, W. H. *J. Phys. Chem*. **1987**, *91*, 5302; Egawa, C.; Nishida, T.; Naito, S.; Tamaru, K. *J. Chem. Soc., Faraday Trans.* **1984**, *80*, 1595; Bradeley, J. M.; Hopkinson, A.; King, D. A. *Surf. Sci.* **1997**, *371*, 255.

(16) Egawa, C.; Naito, S.; Tamaru, K. *Surf. Sci.* **1983**, *131*, 49; Grossman, M.; Loffler, D. G. *J. Catal*. **1983**, *80*, 188; Reed, A. P. C.; Lambert, R. M. *J. Phys. Chem.* **1983**, *88*, 1955.

(17) Choudhary, T. V.; Sivadinarayana, C.; Goodman, D. W. *Catal. Lett.* **2001**, *72*, 197.

(18) Papapolymerou, G.; Bontozoglou, V. *J. Mol. Catal. A* **1997**, *120*, 165.

(19) Purtell, R. J.; Merrill, R. P.; Seabury, C. W.; Rhodin, T. N. *Phys. Rev. Lett.* **1980**, *44*, 1279.

(20) Ali, T.; Walker, A. V.; Klotzer, B.; King, D. A. *Surf. Sci.* **1998**, *414*, 304.

(21) Lauterbach, J.; Schick, M.; Weinberg, W. H. *J. Vac. Sci. Technol. A* **1996**, *14*, 1511.

(22) Hagedorn, C. J.; Weiss, M. J.; Weinberg, W. H. *J. Phys. Chem. B* **2001**, *105*, 3838.

(23) Cornish, J.; Avery, N. *Surf. Sci*. **1990**, *235*, 209; Gardner, P.; Martin, R.; Tushaus, M.; Shamir, J.; Bradshaw, A. M. *Surf. Sci.* **1993**, *287/288*, 135.

(24) Xu, C.; Oh, W. S.; Kim, D. Y.; Goodman, D. W. *J. Vac. Sci. Technol. A* **1997**, *15*, 1261.

(25) Bassignana, I. C.; Wagemann, K.; Kuppers, J.; Ertl, G. *Surf. Sci*. **1986**, *175*, 22.

(26) Redhead, P. A. *Vacuum* **1962**, *12*, 203.

(27) Choudhary, T. V.; Santra, A. K.; Sivadinarayana, C.; Min, B. K.; Yi, C. W.; Davis, K.; Goodman, D. W. *Catal. Lett*., in press.